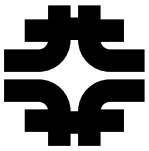

Fermi National Accelerator Laboratory

FERMILAB-Pub-98/296

Muon Collection Channel

A. Van Ginneken and D.V. Neuffer

Fermi National Accelerator Laboratory
P.O. Box 500, Batavia, Illinois 60510

October 1998

Submitted to *Nuclear Instruments and Methods A*

Operated by Universities Research Association Inc. under Contract No. DE-AC02-76CH03000 with the United States Department of Energy

Disclaimer

Distribution

Copyright Notification

Muon Collection Channel

A. Van Ginneken and D. V. Neuffer
*Fermi National Accelerator Laboratory**
Batavia, Illinois 60510

September 17, 1998

Abstract

A preliminary analysis of the collection channel for a muon collider is presented. Pions, produced in a target by 8-30 GeV protons, are captured and transported in a solenoid where they decay into muons. Muon yield and phase space characteristics at the end of the channel can be improved by placing RF cavities and absorbers along the decay channel as well as by providing a supplemental toroidal field in conjunction with the absorbers. Results of Monte Carlo simulations are presented for a few such scenarios.

1 Introduction

Currently there is intense interest in the design of a muon collider. Its basic components, see e.g. [1], are: an 8-30 GeV proton 'driver', pion production target, collection channel, ionization cooling system, muon accelerator, and a storage ring. The purpose of the muon collection channel is to maximize capture of pions produced in the target and—after their decay—maximize the number and phase space density of muons acceptable by the cooling section. Obviously, its design will depend considerably on the designs of both target and cooling systems—and vice versa—so that several iterations will be required to arrive at a definite design. At present the target, collection channel, and cooling system all lack such a definite design. Therefore, in this preliminary analysis of the collection channel, it makes sense to use the same target system throughout the study and to adopt a simple definition of an acceptable muon.

Pion production is simulated using the MARS program[2]. The target is embedded in a high field solenoid to maximize capture of produced particles. Following the target, the solenoidal field is reduced adiabatically as its radius increases. In the long decay channel that follows both the field and radius of

*Work supported by the U. S. Department of Energy under contract No. DE-AC02-76CH03000.

the solenoid are kept constant. In addition to the solenoidal magnetic field, the decay channel must be equipped with RF cavities placed periodically along the length of the channel. Their purpose is to prevent the nascent beam from becoming overly long and—in certain scenarios—to provide some net acceleration.

It may be advantageous to initiate transverse (ionization) cooling at this early stage, i.e., to place a number of 'absorbers' along the channel and to compensate energy losses in them via the RF system. In ionization cooling particles travel through a material medium in which they undergo ionization losses after which they are re-accelerated in RF cavities. The loss occurs parallel to the muon's momentum and thus includes both transverse and longitudinal whereas only the latter gets restored by the RF. However, multiple scattering in the medium 'heats' the beam transversely and the combined processes in the absorber may be approximated by the differential equation [3]:

$$\frac{d\epsilon_N}{ds} = -\frac{1}{\beta^2 E}\frac{dE}{ds}\epsilon_N + \frac{\beta\gamma\beta_\perp}{2}\frac{d\theta_{rms}^2}{ds} \tag{1}$$

where ϵ_N is the transverse normalized emittance, E is the beam energy, dE/ds is the ionization loss rate, β and γ are the usual relativistic kinematics variables, $\beta_\perp$ is the betatron function, and $d\theta_{rms}^2/ds$ is the average rate of growth of the *ms* multiple scattering angle. The ionization losses are subject to fluctuations ('straggling') which predominantly cause heating of the longitudinal emittance which is not included in eq. 1. Location, shape, and composition of these absorbers must be studied as part of any optimization scheme but only low-Z materials need be considered since they perform best in ionization cooling (lower $d\theta_{rms}^2/ds$). The place along the channel where to start introducing absorbers is to be chosen carefully so as to strike a balance between muon cooling and pion losses through inelastic nuclear interactions.

When the muon beam is ready to leave the decay channel its transverse size should preferably be small relative to the solenoid radius. The fringe fields encountered at the solenoid exit increase with radial distance and thus would tend to enlarge an already large beam thereby placing yet stronger demands on the ionization cooling system that follows. It is found that a supplemental toroidal field—in conjunction with the absorbers—can significantly reduce beam size.

It is apparent that in this problem there are a large number of physical parameters which must be specified—within certain bounds of technological feasibility and budgetary constraints—so as to optimize number and phase space density of muons at the end of the channel. This note is a preliminary attempt at such an optimization. These idealized calculations provide a glimpse of what—if anything—may be gained from a given strategy and indicate where more realistic models are worth pursuing. A convenient starting point for this study is the work of H. Kirk et al. as reported in [1].

In the simulation, the long solenoid, cavities, and absorbers are characterized by their location, a common aperture, and by idealized fields. Pion and muon populations propagating through it are analyzed at various stations along the channel, particularly at the exit where total number of muons, their six-dimensional phase space volume, transverse size and phase space volume are the principal figures used for intercomparison.

Sec. 2 briefly describes the models used in the simulation which is followed, in sec. 3, by a sampling of results which illustrate each of the basic features listed above. Concluding remarks are in sec. 4.

2 Calculations

Pion production is calculated using the MARS code [2]. Kaons are neglected in the present study: compared with pions they produce only a small fraction ($\approx$1%) of generally acceptable muons [4]. The target system chosen for the present study is a 36.3 cm long, 1 cm radius gallium target situated on axis in a 20 T solenoid of 7.5 cm radius [1]. The 16 GeV incident proton beam has a Gaussian spread both transversely, $\sigma_x = \sigma_y$ =0.4 cm, and longitudinally, σ_z =30 cm, and is centered on the target. Immediately following the target the field of the solenoid is reduced adiabatically while its radius increases to the value adopted for the decay channel. For most of the results presented here the channel parameters are 15 cm radius, 5 T solenoidal field, and a 203.7 cm long transition solenoid. Some results are included for a channel of 30 cm radius, 1.25 T field and with 403.7 cm for the transition. In the long decay pipe (80-150 m) both solenoidal field and radius are kept constant—even where cavities or absorbers are present.

Simulation of π/μ transport down the decay pipe is considerably simplified. Transport in a plain solenoid between RF cavities and/or absorbers assumes an ideal field: B_z constant throughout and $B_\perp$=0. Particles thus travel along a simple helix from which exit coordinates and momenta are readily obtained and which permits aperture checking along the trajectory. The RF field is represented either by a single boost in energy at mid-gap or by tracing the particle through the gap in a series of small steps. In either case it is assumed to be an ideal electric field: E_z varies sinusoidally in time and $E_\perp$=0. Step-by-step tracing is always performed when a toroidal field is present, with the latter simply superimposed on the solenoidal field.

Muon interactions in absorbers are simulated rather faithfully using the program SIMUCOOL [5]. Pions—in addition to multiple Coulomb scattering and ionization energy losses—may undergo nuclear elastic as well as inelastic interactions. These processes may remove the pion or render it unable to produce an acceptable muon or else the pion remains viable but with a change in momentum. To expedite simulation of pion interactions a special routine is

included. Although it is used for all pions, the routine represents the situation accurately only for relatively low momenta (below ≈600 MeV/c) and for the light nuclides best suited for ionization cooling (hydrogen, lithium, beryllium, and carbon). Production of *extra* pions is neglected since it is improbable for a pion from the sample population to produce a same-charge pion which decays into an acceptable muon. Pion-nucleus interactions therefore reduce to three types: coherent and incoherent scattering, and absorption. Charge exchange is included in the latter since the resulting π^0 is of no further interest. Total cross sections for these processes are taken from experiment [6] for π-momenta up to 440 MeV/c after which they are smoothly joined to the high energy, 'geometrical', cross sections [7]. Parametrization of the angular distribution for incoherent scattering is taken from [8]. Coherent elastic scattering for all nuclear targets is assumed to follow a $d\sigma/dt \propto exp(-80t)$ law where t represents the four-momentum transfer in GeV^2. This is close to experiment at higher energies [9] and, when combined with the parametrization for incoherent scattering, compares well with the data presented in [6]. Pions traversing the absorber are reduced in energy by the *average* ionization energy loss corresponding to their energy with fluctuations neglected. Multiple scattering is assumed to follow the Gaussian approximation. Since one is not engaged here in *pion* ionization cooling these last two assumptions appear justified. It is somewhat unfortunate that the energy region over which pions are collected—dictated mainly by where their production is most copious and where muon ionization cooling is most effective—overlaps considerably with the πN resonance region. In this region, absorption is rather large and the angular distribution for incoherent scattering has a large backward peak in the center of mass. These interactions thus strongly reduce the contribution of the pions to the accepted muon population and therefore absorbers should be inserted only after pion decay is nearly complete.

3 Results

A pion produced muon which has successfully navigated the decay channel is considered acceptable if both its energy and its time of arrival lie within a 300 MeV by 6 m (20 nsec) rectangular window centered in (E–t)-space so as to maximize yield. To facilitate comparisons these widths are identical for all cases presented here. There are no transverse cuts beyond those imposed by the physical aperture of the channel. Although somewhat arbitrary, these limits are meant to represent what is acceptable to the muon cooling stage of the collider. Results quoted here are based on 200,000 protons striking the target while the scatter plots shown below use half that number. Besides total number of muons in the cut (N_μ), their 6-D phase space (ϵ_6), and *rms* projected transverse spatial extent, $\langle x^2 \rangle^{1/2}$, are of considerable interest along with the ratio $N_\mu^2/\sqrt{\epsilon_6}$

which is related to collider luminosity. The 6-D phase space volume quoted here is calculated as the square root of the determinant of the 6-D covariance matrix. Transverse *rms* projected phase space volume ($\langle\epsilon_T^2\rangle^{1/2}$) refers to the fourth root of the determinant of the 4-D x-p_x-y-p_y covariance matrix to account for $x - p_y$, $y - p_x$ coupling introduced by the solenoidal field. Where quoted below, these results always refer to muons within the cut. Sensitivity to a few large-amplitude particles poses problems, especially in limited-statistics Monte Carlos, so that uncut (or too widely cut) phase space volumes lack robustness.

All simulations reported here consider π^+/μ^+ only. If the same channel is used to collect μ^+ and μ^-, it seems advantageous to optimize settings for μ^-. The same settings then also serve collect μ^+, but with the E_z of the cavities reversed in sign, on the next pulse. Since—in most models—π^+ production slightly exceeds that of π^- this strategy will tend to equalize their numbers. Trial runs performed in this fashion actually still retain a slight excess of positives.

3.1 Cavities Only

A set of RF cavities is characterized by their number, location, (peak) electric field, frequency, and timing. An iterative procedure is developed along which convergence is pursued to some (local) maximum of muons captured and of phase space density in this parameter space. However, many such local maxima may exist and it remains to discover the one best suited overall. For now this is decided on the basis of simple criteria such as the ones employed here but eventually these should be broadened to include those of a more practical nature. Optimum RF frequency is closely related to bunch width (standard deviation) of the πs and μs at a given cavity location. At each step of the iteration, and for each cavity, a new frequency may thus be estimated for use in the next run—even though an economical design will have several sets of cavities at the same frequency. Timing of the RF is likewise related to the average time of arrival and is changed between iterations.

For a suite of cavities composed of sets with identical parameters the models used here tend to confirm the results of Kirk et al. [1]. Because the initial pion population here—taken from MARS simulations—is completely different from the flat spectra used in [1], quantitative comparisons are not attempted. A simple sine-wave RF field as in [1] appears not well matched to the shape of the π/μ bunch in (E–t)-space. Since bunch shape changes relatively slowly between adjacent cavities this may be improved upon by matching to a combination of two sine-waves from two such cavities, where one is free to vary amplitude, frequency, and phase difference of the waves. Obviously, this scheme could be extended to multiple cavities—although the constant bunch shape assumption becomes more questionable with each addition—but such an exercise is perhaps best left to more realistic simulations. Future work may also consider multi-

harmonic cavities for even better matching to bunch shape.

The channel is almost 80 m long and contains a total of 65 cavities—one every 1.2 m. A crude optimization, carried out with only cavities present, points to the parameters displayed in table 1. The timing of the cavities is adjusted individually during iteration. Early on in the iteration these tend to be simply the average arrival time of those μ/π which produce an accepted μ at channel exit, while in later stages variations with respect to this average time are introduced. In view of the large number of parameters to be varied, a complete exploration is not attempted.

For the 5 T/15 cm channel fig. 1 shows bunch shape in energy-time space at various distances along the channel. Both πs and μs are present in fig. 1. Superimposed on each plot is the variation with time of the energy gain averaged over two adjacent cavities (scale on right ordinate). Fig. 2 is similar but is restricted to those μs, plus their π progenitors, eventually accepted at the exit. For the 15 cm channel with 5 T field a total number of 0.349 muons per proton on target are accepted in the 20 nsec-by-0.3 GeV region. (For comparison a combined total of 0.700 pions and muons per proton pass through the transition solenoid.) Their normalized 6-D phase space measures 225 cm^3 with *rms* energy spread of 72 MeV centered at about 350 MeV. Normalized *rms* tranverse phase space measures 1.63 cm and *rms* projected beam size is 4.85 cm. Fig. 3 portrays the transverse shape of the (uncut) bunch at the same points along the channel as in figs 1 and 2.

For the 1.25 T/30 cm channel with the same parameter set (table 1), but with timings re-optimized, a total of 0.287 muons per proton are accepted *versus* 0.487 muons-plus-pions passing through the transition solenoid. Normalized 6-D phase space is 257 cm^3 with *rms* energy spread of 78 MeV centered at 307 MeV. Normalized *rms* tranverse phase space measures 1.73 cm and *rms* projected transverse size is 10.12 cm. The larger radius, lower field decay tube thus results in about 18% fewer muons collected with about 14% larger 6-D emittance and a beam size roughly twice as large compared with the 15 cm, 5 T version.

3.2 Absorbers

A set of absorbers is determined by their number, size, shape, and material composition. Along with these new parameters the old ones, listed for the cavities-only case above, may need to be readjusted. When such absorbers are present acceleration must be provided to compensate for energy loss by the muons. In the simulation field strength, frequency, and phase of adjacent cavities are manipulated so that at the center of the bunch such compensation is almost exact and exhibits a rather flat time dependence. On either side of this plateau there is net stabilizing acceleration: positive for lagging–, negative for speeding particles. Below about 150 MeV kinetic energy—where a substan-

Table 1: Maximum total acceleration in MeV per meter, frequency in MHz, and phase shift in radians for each cavity (serial number in leftmost column) for cavities-only case. Each cavity is 1.2 m long.

		acc	27.00	9.00	25.20	8.40	23.40	7.80
1	- 6	freq	90.00	180.00	70.00	140.00	60.00	120.00
		phase	0.00	2.20	0.00	2.20	0.00	2.20
		acc	21.60	7.20	19.80	6.60	18.00	6.00
6	-12	freq	54.00	108.00	48.00	96.00	44.00	88.00
		phase	0.00	2.20	0.00	2.20	0.00	2.20
		acc	17.10	5.70	16.20	5.40	15.30	5.10
13	-18	freq	42.00	84.00	40.00	80.00	39.00	78.00
		phase	0.00	2.20	0.00	2.20	0.00	2.20
		acc	14.40	4.80	13.50	4.50	12.60	4.20
19	-24	freq	37.00	74.00	35.00	70.00	34.50	69.00
		phase	0.00	2.20	0.00	2.20	0.00	2.20
		acc	11.70	3.90	10.80	3.60	10.80	3.60
25	-30	freq	34.00	68.00	33.50	67.00	33.00	66.00
		phase	0.00	2.20	0.00	2.20	0.00	2.20
		acc	10.80	3.60	10.80	3.60	10.80	3.60
31	-36	freq	32.50	65.00	32.00	64.00	31.50	63.00
		phase	0.00	2.20	0.00	2.20	0.00	2.20
		acc	10.80	3.60	10.80	3.60	10.80	3.60
37	-42	freq	31.00	62.00	30.00	60.00	28.00	56.00
		phase	0.00	2.20	0.00	2.20	0.00	2.20
		acc	10.80	3.60	10.80	3.60	10.80	3.60
43	-48	freq	27.00	54.00	26.00	52.00	25.00	50.00
		phase	0.00	2.20	0.00	2.20	0.00	2.20
		acc	10.80	3.60	10.80	3.60	10.80	3.60
49	-54	freq	25.00	50.00	25.00	50.00	25.00	50.00
		phase	0.00	2.20	0.00	2.20	0.00	2.20
		acc	10.80	3.60	10.80	3.60	10.80	3.60
55	-60	freq	25.00	50.00	25.00	50.00	25.00	50.00
		phase	0.00	2.20	0.00	2.20	0.00	2.20
		acc	10.80	3.60	10.80	3.60	10.80	
61	-65	freq	25.00	50.00	25.00	50.00	25.00	
		phase	0.00	2.20	0.00	2.20	0.00	

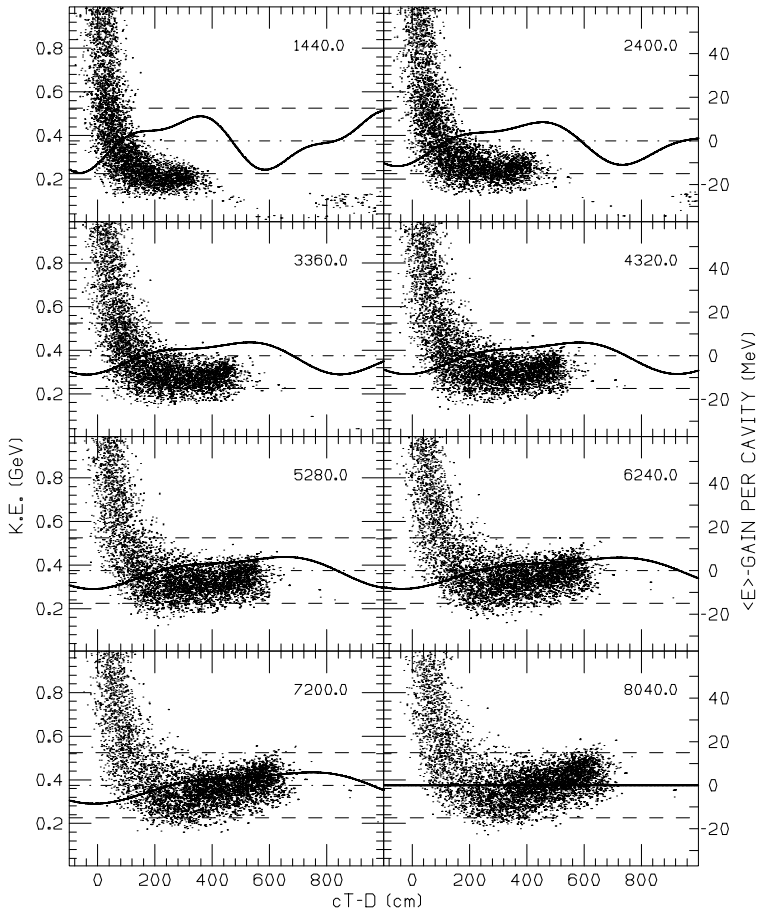

Figure 1: Evolution of longitudinal phase space for cavities-only case. Distance from target (in cm) is in upper right corner of each plot. Curves show acceleration averaged over adjacent cavities (right scale).

tial fraction of the pions are captured—ionization losses decrease sharply with energy causing the absorbers to contribute to a progressive widening of the energy spread of the bunch. Above minimum ionization—at about 300 MeV—the situation reverses and becomes at least marginally stable (if fluctuations are ignored). It is therefore advantageous to provide some net acceleration to the bunch prior to impinging on the absorbers so as to avoid the regime below 150 MeV.

So far only absorbers composed of lithium hydride (density=0.82 g/cm^3, minimum dE/dx=1.56 MeV/cm—at about 300 MeV kinetic energy [7, 10]) are studied in the simulations. Other candidates should be considered and one is obviously not limited to one and the same material throughout. For the absorbers-only case only straight cylindrically shaped absorbers have been

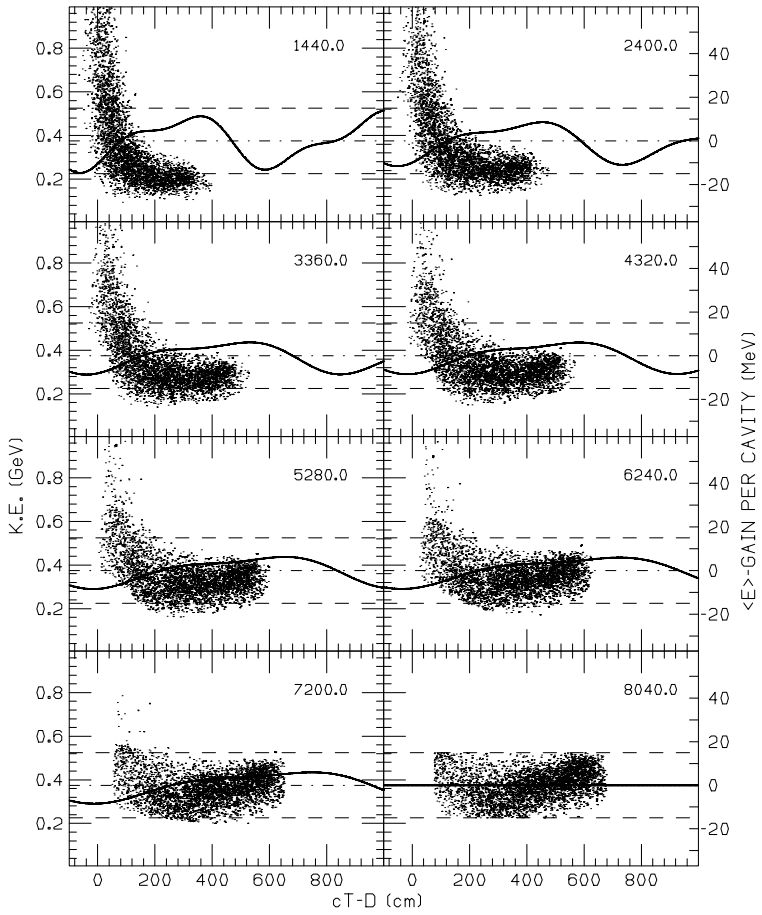

Figure 2: Evolution of longitudinal phase space for cavities-only case. Only accepted muons and pion progenitors are shown. Distance from target (in cm) is in upper right corner of each plot. Curves show acceleration averaged over adjacent cavities (right scale).

simulated. More complicated shapes may offer advantages—particularly when combined with a toroidal magnetic field (see below) or with a radially varying RF field.

Because the absorbers-plus-RF provide some cooling it may be advantageous to lengthen the channel beyond where new muons are created in significant numbers so as to minimize losses when exiting the solenoid. In the results presented here the decay pipe is 146.4 m long and contains 121 cavities, 1.2 m apart, along with 60 absorbers, each of lithium hydride 10 cm thick, placed in the downstream half of the channel beginning at 74.5 m. Table 2 shows—in the manner of table 1—accelerations, frequencies, and phase shifts for cavities 61–90. Cavities 1–60 are identical to table 1. After the 86th cavity the same pattern repeats until the end.

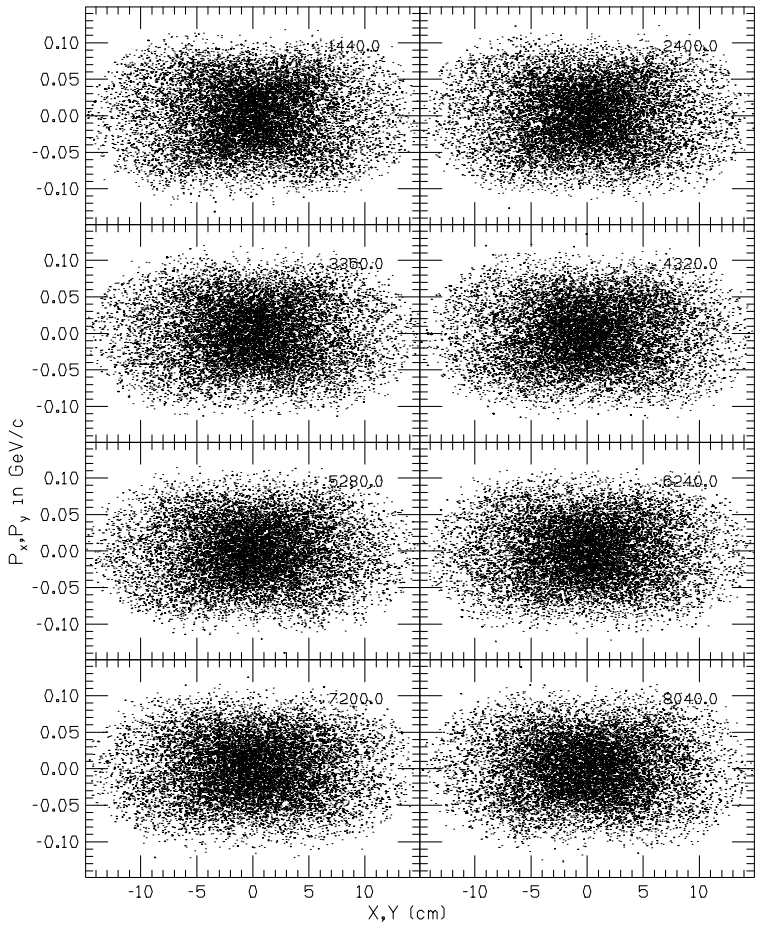

Figure 3: Evolution of transverse phase space for cavities-only case. Distance from target (in cm) is in upper right corner of each plot.

Results for the 5 T/15 cm channel are shown in figs. 4–6 in the fashion of figs. 1–3 without repeating the front of the channel which is identical—prior to the absorbers—for figs. 1 and 4 as well as for figs. 3 and 6. Not quite the same relation exists between figs. 2 and 5 since the selection made at the end of the channel—after traversing the absorbers—dictates what is included in the front part. Nonetheless, prior to the absorbers there is little difference between the two cases. At the exit 0.302 muons per proton on target are accepted in the 20 nsec-by-0.3 GeV cut. Evidently, scattering and straggling in the absorbers cause some loss of particles. Normalized 6-D phase space measures 63 cm^3 with an *rms* projected transverse size of 4.45 cm. Particle losses likely account for most of the reduction in beam size observed vis-a-vis the cavities–only case (about 2% loss is expected from μ-decay). A three– to fourfold reduction in phase space is observed. As is clear from fig. 6 this is

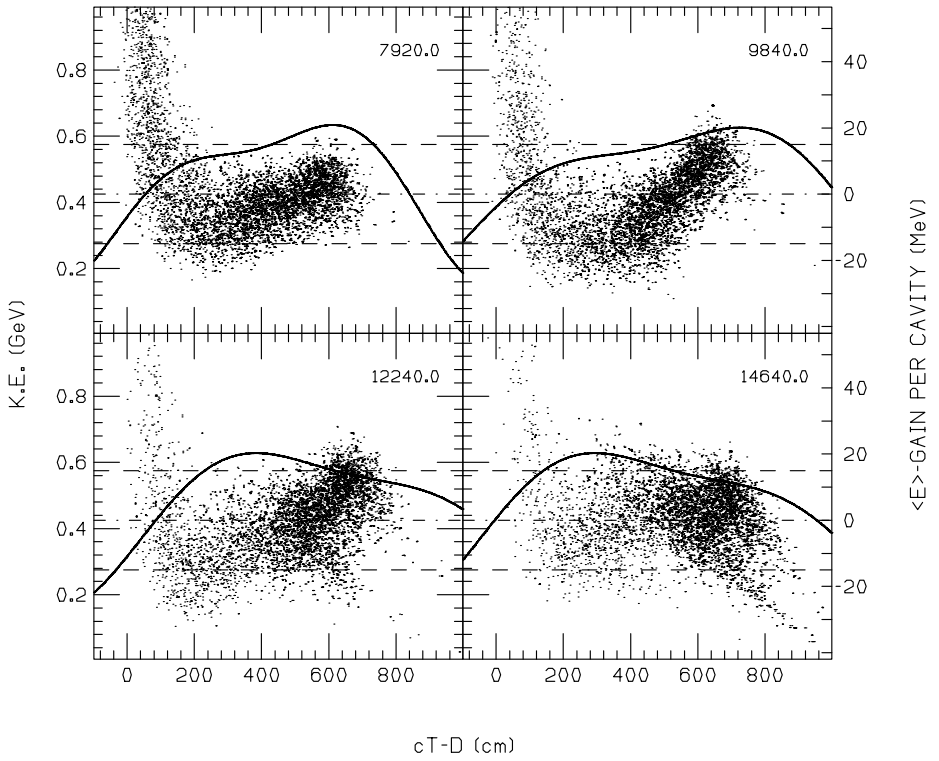

Figure 4: Evolution of longitudinal phase space with absorbers present. Distance from target (in cm) is in upper right corner of each plot. Curves show acceleration averaged over adjacent cavities (right scale). Phase space prior to 74.5 m is as depicted in fig. 1.

mostly due to the reduction in transverse momentum along with some due to particle losses. The *rms* transverse phase space is reduced to 0.91 cm while the average kinetic energy is 407 MeV with a spread of 68 MeV. By the $N_\mu^2/\sqrt{\epsilon_6}$ standard there is a gain of over 37% when absorbers are present.

For the 1.25 T/30 cm channel the same parameters as in tables 1 and 2 are used, except for one necessary adjustment: all odd numbered cavities are at a $\pi/2$ phase differential with respect to the evens. Timings are also re-optimized. Results for the wider channel are much less favorable: 0.130 muons per proton are collected. This means that—with decay subtracted—the absorbers cause 53% of the muons to get lost *versus* less than 11% in the higher field channel. These larger losses are likely due to muon scattering in the absorbers. For given p_T the Larmor radius is four times larger while the channel radius is only twice that of the narrower one. A scattering event—especially one occurring near the periphery of the channel—is thus much more likely to wipe out the muon. The difference between the cooling channels may be verified from the differential equation for transverse cooling, eq. 1, which—for lithium hydride

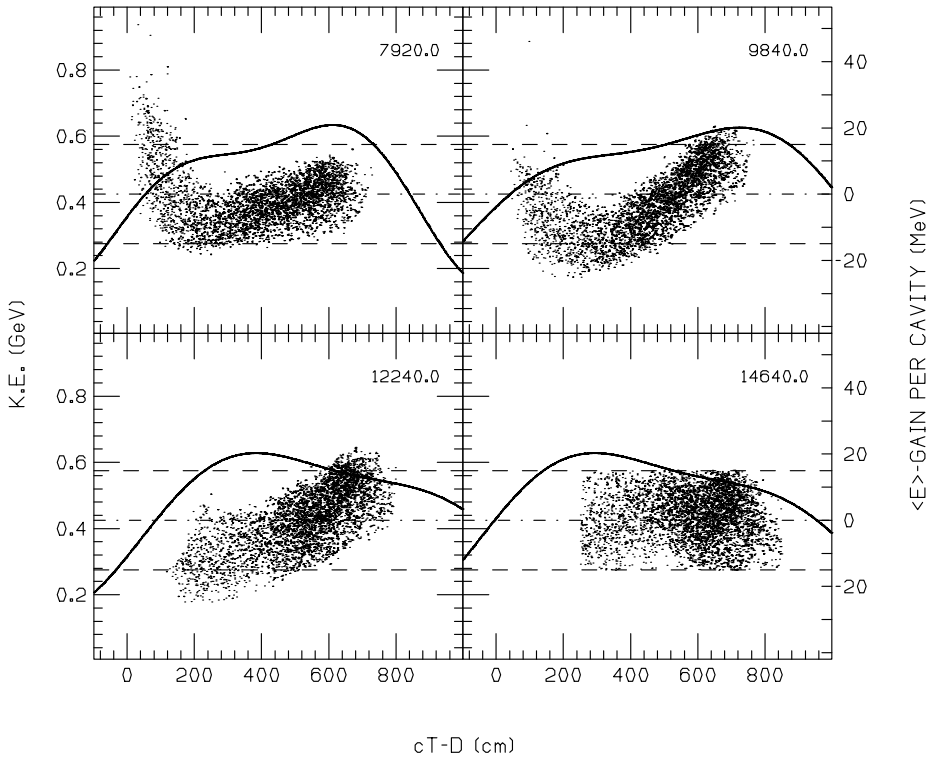

Figure 5: Evolution of longitudinal phase space with absorbers present. Only accepted muons and pion progenitors are shown. Distance from target (in cm) is in upper right corner of each plot. Curves show acceleration averaged over adjacent cavities (right scale). Phase space prior to 74.5 m is *approximately* as depicted in fig. 2.

absorbers—may be written as:

$$\frac{d\epsilon_N}{ds} \simeq -\frac{1}{p}\frac{dp}{ds}\left(\epsilon_N - 0.007\frac{\beta_\perp}{\beta}\right). \qquad (2)$$

In beam transport through solenoids, the matched betatron function $\beta_\perp$, in units of meters, is conveniently written as $\beta_\perp = 2p/0.3B$ with the momentum, p, in GeV/c and the magnetic field, B, in Tesla. Thus, at p=0.45 GeV/c, in the 5 T solenoid $\beta_\perp$=0.6 m while the 1.25 T channel has $\beta_\perp$=2.4 m. (These values match approximately the betatron function derived from beam size $\beta_\perp = \sigma_x^2/\epsilon_\perp$—where σ_x is the projected transverse *rms* beam size and $\epsilon_\perp$ is the unnormalized transverse emittance—at the beginning of the absorber section.) Eq. 2 shows that net cooling requires $\beta_\perp <\sim 2$ m for ϵ_N= 1.4 cm which prevails for the 5 T solenoid but not for the 1.25 T case. The *rms* equations thus confirm what is seen in the simulations: cooling in the 5 T channel and beam loss from excess heating at 1.25 T.

Normalized 6-D phase space is 271 cm^3—a slight increase from the no-

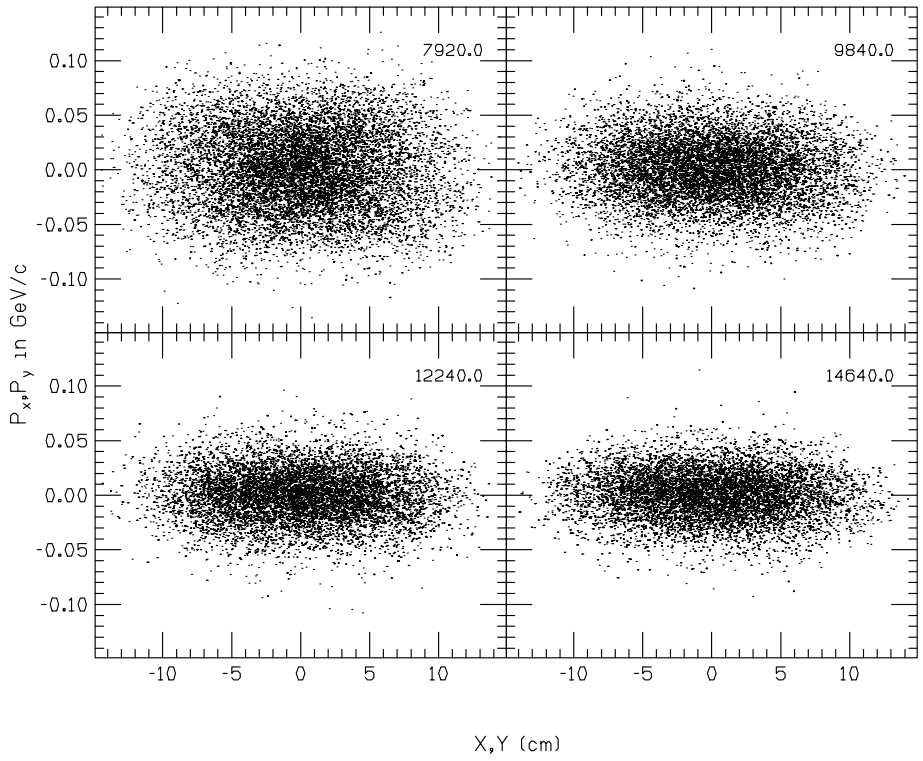

Figure 6: Evolution of transverse phase space with absorbers present. Distance from target (in cm) is in upper right corner of each plot. Phase space prior to 74.5 m is as depicted in fig. 3.

absorber case. In view of the large losses this actually represents strong net heating. The energy distribution is centered at about 475 MeV with a spread of 62 MeV. Normalized *rms* transverse phase space at 1.81 cm has changed very little and projected transverse size has grown to 11.17 cm. This growth tends to support the conclusion that the losses occur mainly when muons acquire larger Larmor orbits. Figs. 7 and 8 show the development of longitudinal and transverse phase space for this case. Both losses and 6-D phase space volume are smaller at upstream locations. However, it appears unlikely that much can be gained by running the wider channel equipped with just plain absorbers.

3.3 Toroidal Fields

When absorbers are included, cooling results mainly by reducing the aggregate p_T of the beam with little change in transverse size. Since small transverse size is advantageous when exiting the solenoid, some focusing in the decay pipe—prior to exiting—becomes desirable. One method proposed here is to provide a supplemental (focusing) toroidal field which impels the particles toward the

Table 2: Maximum total acceleration in MeV per meter, frequency in MHz, and phase shift in radians for each cavity (serial number in leftmost column) with absorbers present. Cavities 1–60 are as in table 1, for 91-121 the last row is repeated.

		acc	37.50	12.39	37.50	12.39	37.50	12.39
61	- 66	freq	24.00	48.00	23.00	46.00	22.00	44.00
		phase	0.94	4.02	0.94	4.02	0.94	4.02
		acc	37.50	12.39	37.50	12.39	37.50	12.39
67	- 72	freq	21.00	42.00	20.00	40.00	19.00	38.00
		phase	0.94	4.02	0.94	4.02	0.94	4.02
		acc	37.50	12.39	37.50	12.39	37.50	12.39
73	- 78	freq	18.00	36.00	18.00	36.00	18.00	36.00
		phase	0.94	4.02	0.94	4.02	0.94	4.02
		acc	37.50	12.39	37.50	11.25	37.50	11.25
79	- 84	freq	18.00	36.00	18.00	36.00	18.00	36.00
		phase	0.94	4.02	0.94	4.02	0.94	4.02
		acc	37.50	11.25	37.50	11.25	37.50	11.25
85	- 90	freq	18.00	36.00	18.00	36.00	18.00	36.00
		phase	0.94	2.83	0.94	2.83	0.94	2.83

center of the channel. Such a field may be created by a wire running down the center of the channel or better by a set of wires which together form part of a cylindrical surface centered on axis. The particles now orbit about the center of the pipe when viewed along the its axis. A small toroidal field causes the Larmor motion to precess about the center of the pipe but when the field (or the muon's p_z) gets larger the orbits become more complicated and motion about the center begins to dominate the Larmor motion. Upon traversing an absorber-plus-restoring-RF the particles lose some p_T which shrinks the orbit about the center, thereby providing some net focusing (along with the cooling).

In the simulation the material presence of any wires is neglected with only the field presumed to be there. In practice the wires will have to be brought into and out of their locations near the center of the channel so as to stay clear of the cavity gaps. This might best be done at the location of the absorbers where mechanical support for the wires can be readily provided. The field created by the current in these return wires is also neglected in this calculation. Having many wires which fan out from near center to the circumference of the pipe helps reduce the magnetic field close to a wire. Effects of crossing near the feed wires are lessened by fact that a muon encounters opposing fields upon leaving a cavity and entering the next. In the simulation the gap itself is represented by a simple kick delivered over zero length so the toroidal field is simply taken to be continuous. Muon interactions in the wires may have deleterious effects on beam phase space which are not investigated here. However, these effects may

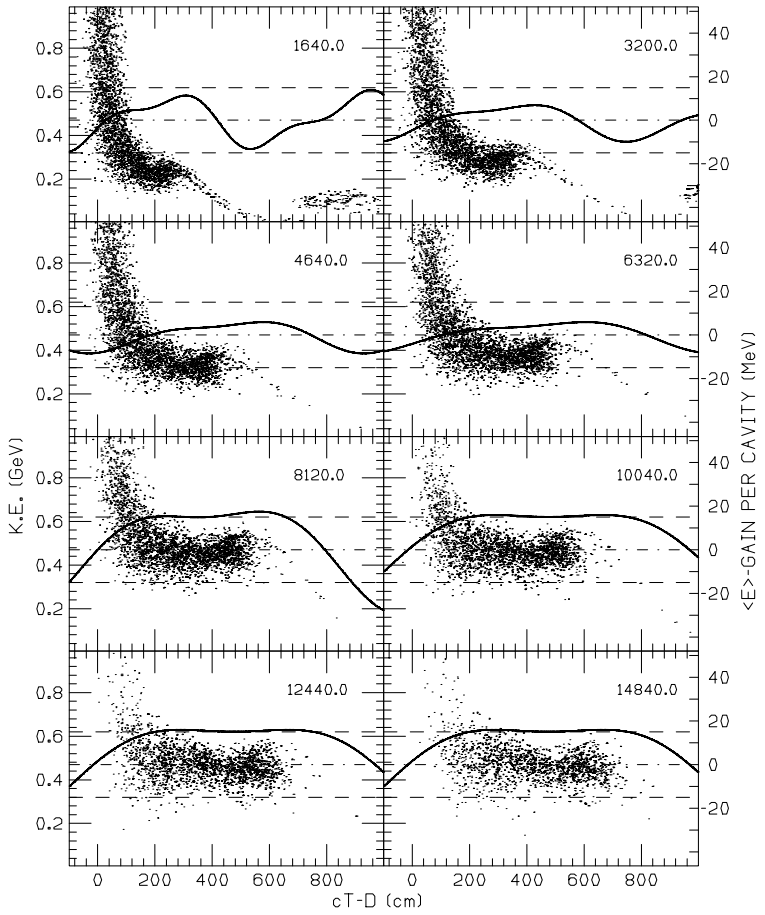

Figure 7: Evolution of longitudinal phase space with absorbers present for *wide channel*. Distance from target (in cm) is in upper right corner of each plot. Curves show acceleration averaged over adjacent cavities (right scale).

be offset by shaping the absorber, e.g., by reducing the material in the radial region where wires are present. A sample of results showing dependence on absorber shape is included below. As represented in the calculation then, the field is generated by a current running along an infinitesimally thin concentric cylinder of radius, r_{cyl}, so as to produce a toroidal field of specified strength. For convenience this field is always quoted below at a *reference radius of 1 cm.* For $r > r_{cyl}$ the field is assumed to decline as $1/r$ while it vanishes inside r_{cyl}. Note that, for almost all results quoted here, $r_{cyl} > 1$ cm and the field actually vanishes at the reference radius.

For the results presented here, input parameters are kept very close to the previous case of absorbers without toroidal field so as to facilitate comparison. Cavities and absorbers are the same in number and placement and with settings

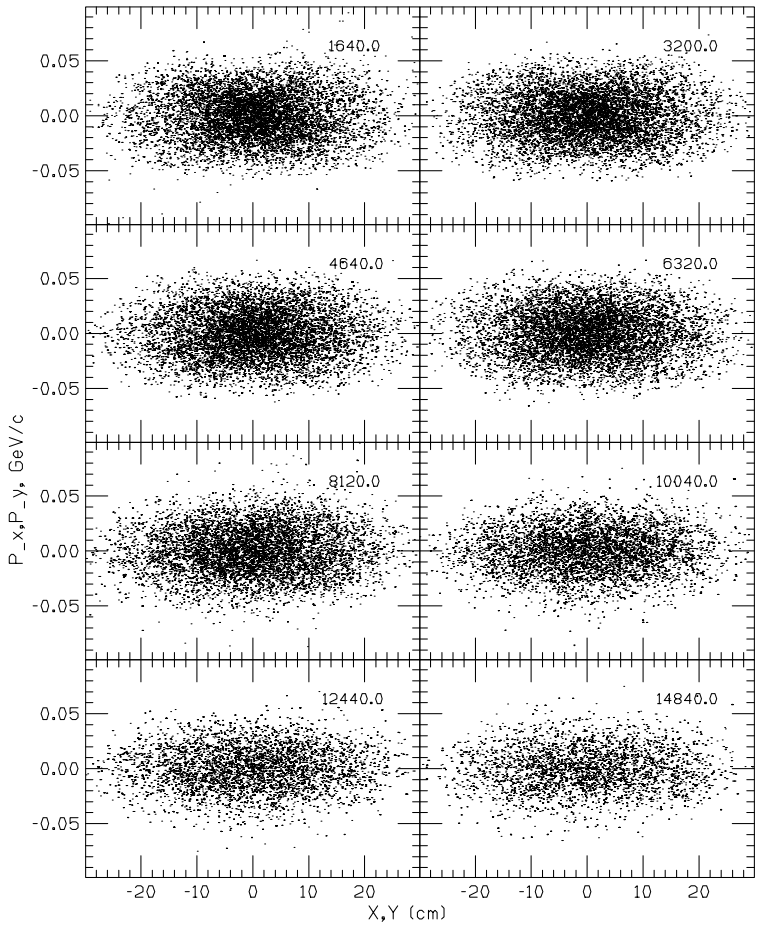

Figure 8: Evolution of transverse phase space with absorbers present for *wide channel*. Distance from target (in cm) is in upper right corner of each plot.

as in tables 1 and 2. The toroidal field begins 4.8 m (four cavities) before the absorbers. Modifications in shape of the absorbers are examined: instead of a flat cylinder a combination cylinder-plus-cone is used. Total thickness at the center is maintained at 10 cm: thus a cone height of 2 cm specifies an 8 cm thick flat cylinder adjoined by a cone with base matched to the cylinder and 2 cm in height. The toroidal field need not be the same throughout. So far the only variant which has been explored is to keep field strength constant but shrink the cylinder radius linearly with distance along the pipe thus shrinking the near-axis no-field region.

Figs. 9–11 present results in the manner of figs. 4–6 for the narrow channel case where the (current carrying) cylinder starts at 5 cm radius at 69.6 m along the pipe and shrinks down to 3 cm at the exit (146.4 m). The remarks made in comparing figs. 4–6 to figs. 1–3 apply here also. The field is specified as 2 T at

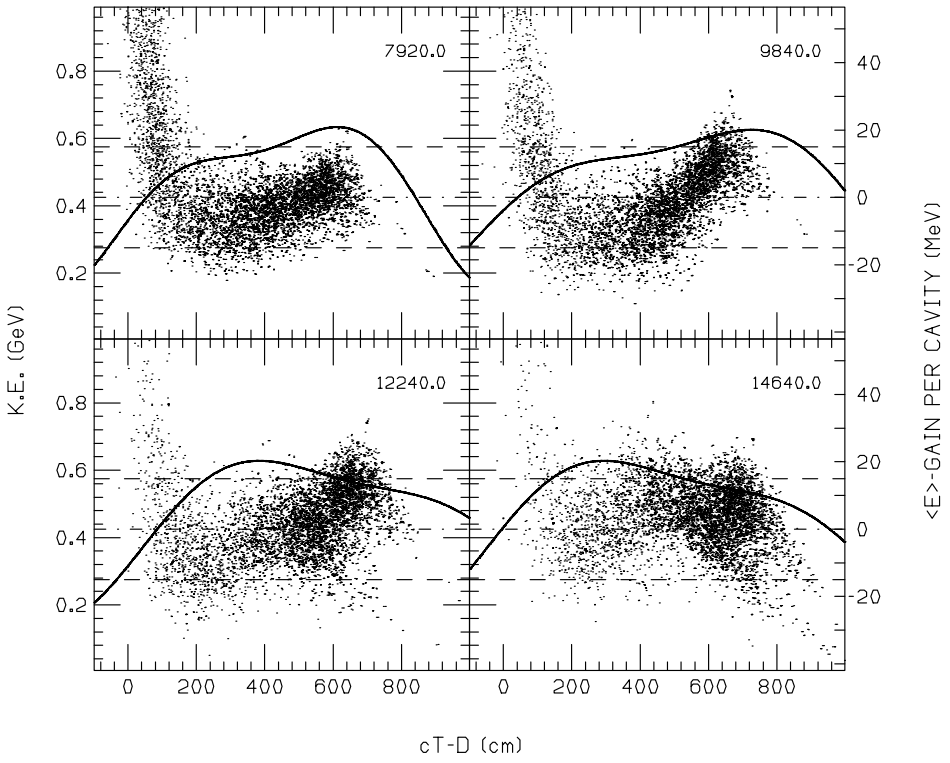

Figure 9: Evolution of longitudinal phase space for absorbers-plus-toroids. Distance from target (in cm) is in upper right corner of each plot. Curves show acceleration averaged over adjacent cavities (right scale). Phase space prior to 69.6 m is as depicted in fig. 1.

1 cm which means that the highest field encountered here is 2/3 T at a radius of 3 cm at the exit. Total number of muons in the common 6 m by 300 MeV cut is 0.324 while the 6-D phase space measures 63 cm^3. Projected *rms* transverse size is 3.06 cm and *rms* transverse phase space area is 0.86 cm. The muons have average kinetic energy of 480 MeV with *rms* spread of 72 MeV. Fig. 12 shows final longitudinal phase space with projections onto the time and energy axes. While the emitttance is practically unchanged from the plain absorbers case there is a marked increase in number of muons captured and a strong decrease in beam size (by about 31%). The two effects are no doubt related since smaller beam size lessens the chance of a muon being lost by a change in radial excursion due to interactions in an absorber. This can be seen graphically by comparing figs. 6 and 11.

Comparable results for the wide channel are not pictured here but show a much more dramatic recovery of the number of muons captured when a toroidal field is applied. For the case of flat absorbers and a current carrying cylinder of r=12 cm at the start (z=69.6 m) and r=6 cm at the exit with a 2.5 T

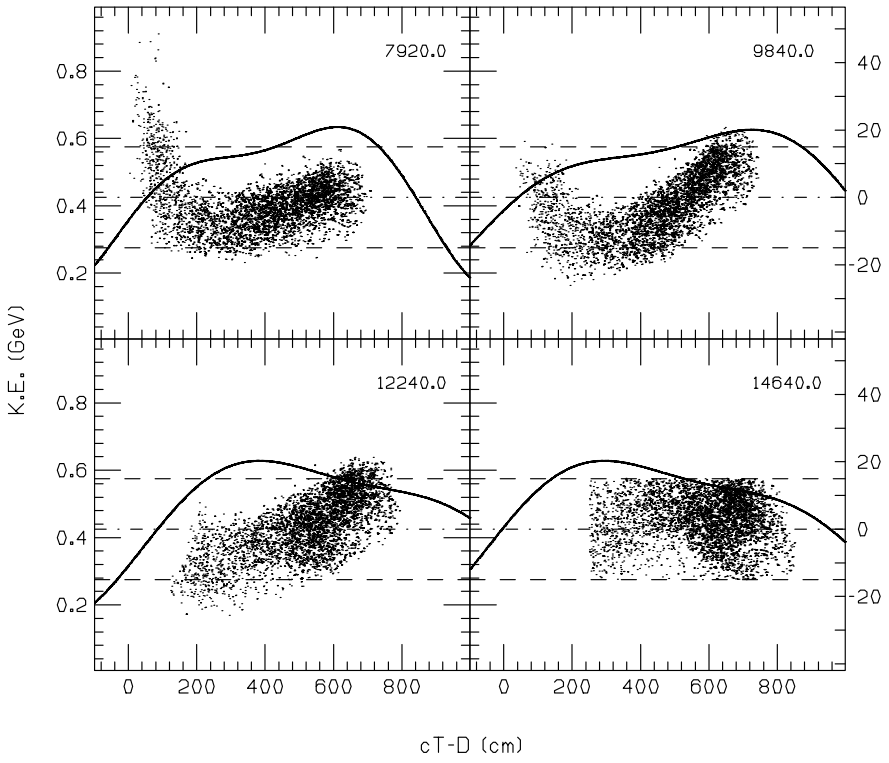

Figure 10: Evolution of longitudinal phase space for absorbers-plus-toroids. Only accepted muons and pion progenitors are shown. Distance from target (in cm) is in upper right corner of each plot. Curves show acceleration averaged over adjacent cavities (right scale). Phase space prior to 69.6 m is *approximately* as depicted in fig. 2.

reference field at 1 cm there are 0.258 muons in the cut with a 6-D phase space volume of 153 cm^3, *rms* transverse phase space of 1.36 cm and an *rms* projected size of 5.02 cm. Thus number of muons is roughly doubled while 6-D emittance and beam size are halved from the no-toroidal-field case. This case also compares favorably to the one without absorbers: even though number of muons captured is about 10% less and $N_\mu^2/\sqrt{\epsilon_6}$ is nearly unchanged, beam size, ϵ_6, and transverse emittance are all down substantially. The toroidal fields substantially modify the analysis in terms of the *rms* equations which compared the 5 T and 1.25 T channels with plain absorbers. Since the toroidal field adds focusing $\beta_\perp$ is reduced, particularly in the 1.25 T channel, and some cooling is obtained in both cases without excess beam losses.

Table 3 summarizes the main results for the various simulations performed here. Note the contrast between $\langle\epsilon_T^2\rangle^{1/2}$ and $\epsilon_x(=\epsilon_y)$. For the empty channel it shows strong coupling which almost disappears when absorbers are present. Note also that the 'bottom line', $N_\mu^2/\sqrt{\epsilon_6}$, may change considerably after the

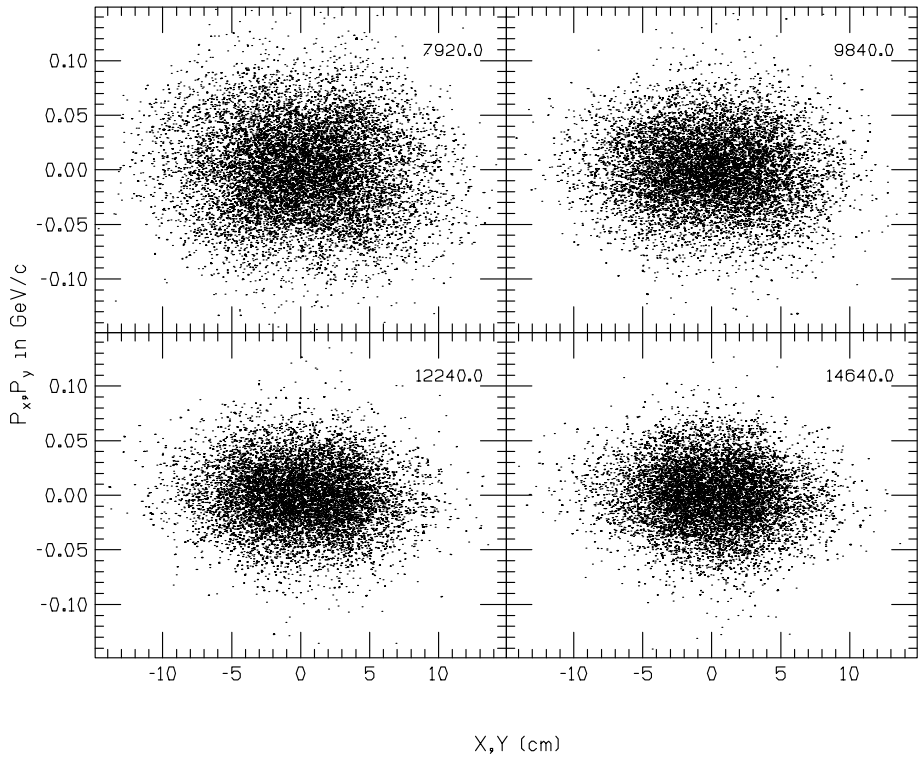

Figure 11: Evolution of transverse phase space for absorbers-plus-toroids. Distance from target (in cm) is in upper right corner of each plot. Phase space prior to 69.6 m is as depicted in fig. 3.

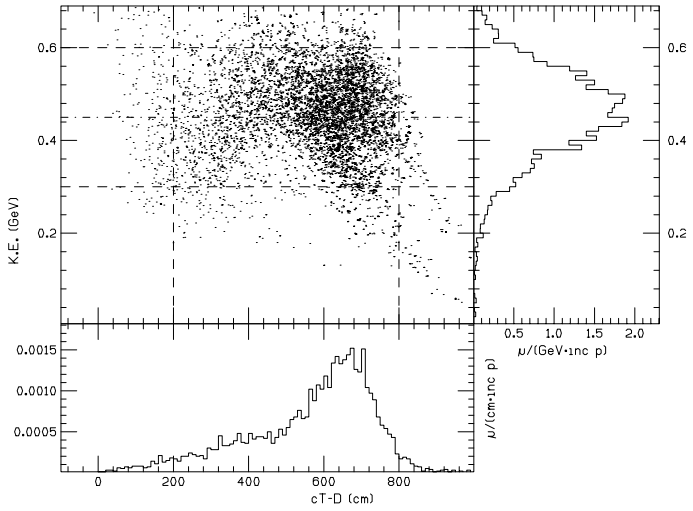

Figure 12: Final longitudinal phase space with projections for absorbers-plus-toroids.

Table 3: Summary of simulation results (see text for details).

	no absorbers		*absorbers*		*+toroidal field*	
$R_{sol}, cm/B_{sol}, T$	15/5	30/1.25	15/5	30/1.25	15/5	30/1.25
N_μ	0.349	0.287	0.302	0.130	0.324	0.258
ϵ_6, cm^3	225	257	63	271	63	153
$\langle\epsilon_T^2\rangle^{1/2}, cm$	1.63	1.73	0.91	1.81	0.86	1.36
ϵ_x, cm	2.18	2.08	0.92	2.11	0.89	1.37
$\langle x^2\rangle^{1/2}, cm$	4.85	10.12	4.45	11.17	3.06	5.02
σ_E, MeV	72	78	68	62	72	61
$\langle E_{kin}\rangle, MeV$	350	307	407	475	480	484
$N_\mu^2/\sqrt{\epsilon_6}, cm^{-3/2}$	0.0081	0.0051	0.0115	0.0010	0.0132	0.0054

muons exit the solenoid—where small $\langle x^2\rangle^{1/2}$ is expected to cause less disruption

It is of interest to look briefly what happens when some of the above parameters are varied one-at-a-time—without launching into a full exploration of the parameter space. The basic parameter set for both narrow and wide channel are kept the same as above except for the one being varied.

• Fig. 13 shows number of muons captured and *rms* radius of the bunch along with 6-D normalized phase space and its longitudinal component as the applied toroidal field varies from 0 to 4 T. The abcissa of fig. 13 gives the toroidal magnetic field strength at 1 cm radius where, in fact, no field is present. Thus the largest field encountered here is at 3 cm radius where it varies from 0 to 4/3 T in the narrow– and from 0 to 2/3 T at 6 cm in the wide channel. Particularly in the wide channel case, the marked decrease in beam size might permit a smaller solenoid radius in the later stages.

• In fig. 14 the same type of results are presented when the reference field is kept at 2 T while the exit radius of the current carrying cylinder in the narrow channel varies from 0.5 to 5 cm (at 69.6 cm) and from 1 to 10 cm in the wide case. Placing the current carrying wires closer than about 2 cm to the center of the pipe (narrow channel) or 4 cm (wide channel) increases the angular spread of the beam without concomitant reduction in size, causing the larger emittances observed at small R_{exit}.

• With the exit radius fixed at 2 cm and 6 cm, respectively for the narrow and wide channels, the starting radius is now varied leading to the situation depicted in fig. 15. In both cases there is a broad middle region from which to choose R_{start} for efficient collection.

• The effects of absorber shape are examined. Thickness at the center is kept at 10 cm but cone height (ΔW) is varied from 0 (flat cylinder 10 cm thick) to 4 cm (flat cylinder 6 cm thick plus cone 4 cm high at center). Especially for

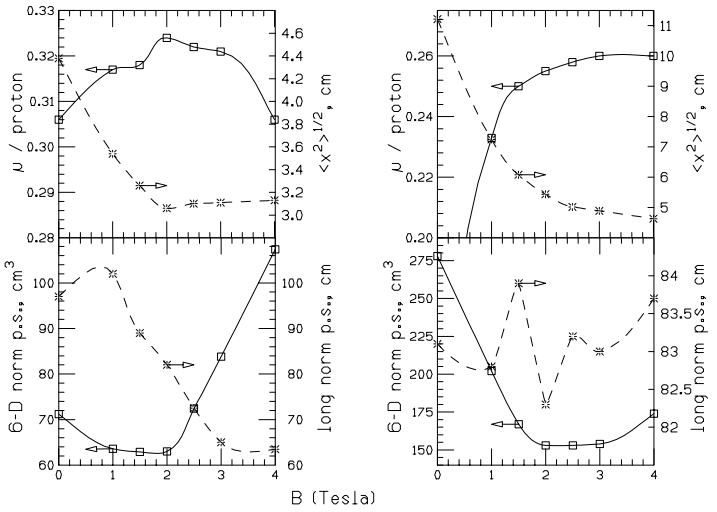

Figure 13: (**top**) Number of muons captured (*left scale*), *rms* radius (*right scale*) and (**bottom**) normalized 6-D (*left scale*) and longitudinal phase space (*right scale*) vs (toroidal) magnetic field strength at 1 cm. Figures on **left** refer to 5 T, 15 cm radius solenoidal channel with radius of current carrying cylinder changing from 5 cm at 69.5 m to 3 cm at 146.4 m (exit) and with absorbers 10 cm thick at center, 8 cm at pipe radius. Figures on **right** refer to 1.25 T, 30 cm radius solenoidal channel with radius of current carrying cylinder changing from 12 cm at 69.5 m to 6 cm at 146.4 m (exit) and with flat 10 cm thick absorbers.

the narrow channel, one sees from fig. 16 that some extra material at smaller radii may actually be desirable. More importantly, in both cases results appear fairly insensitve to ΔW. Therefore one can reasonably expect that the effects of muon trajectories intersecting the wires will not make application of toroidal fields unmanageable. The presence of the central wires adds more material at lower radii. Whatever the wire cross section (assumed infinitesimal here) may be in a practical design, the muons' Larmor motion will effectively spread it over a larger area of the beam. More precise work should explicitly include the wires and then optimize absorber shape in their presence. The return wires—both the material and the fields generated by them—must likewise be taken into account. As already mentioned, strong effects due to the fields are not anticipated and by attaching the return wires to the absorbers one may compensate for their material presence by providing less absorber material there.

It is clear from lack of smoothness of the (interpolating) curves in figs. 13–16 that significant statistical error is present in the results although certain trends are clearly established. In the above exercises, the 20 nsec-by-0.3 GeV cut in (E–t)-space is placed so as to maximize muon yield but with rather coarse grained variation. Phase space volume, beam size, etc., will also be influenced by this placement. In addition to statistical error, these numbers thus acquire

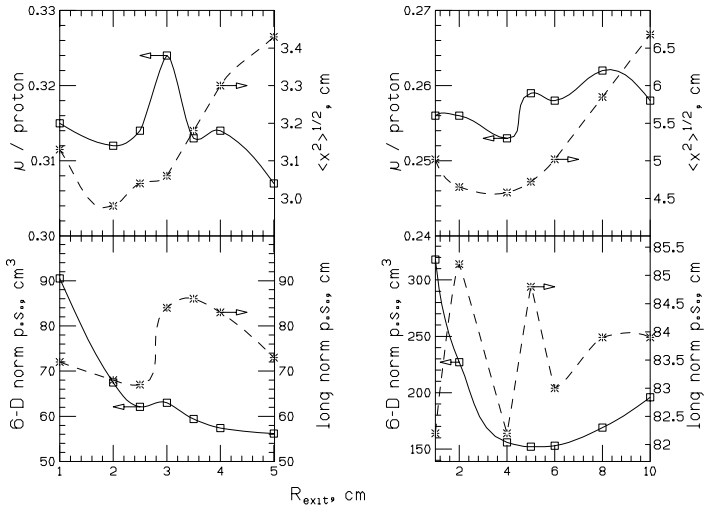

Figure 14: (**top**) Number of muons captured (*left scale*), *rms* radius (*right scale*) and (**bottom**) normalized 6-D (*left scale*) and longitudinal phase space (*right scale*) vs radius of current carrying cylinder at exit. Figures on **left** refer to 5 T, 15 cm radius solenoidal channel with 5 cm radius of current carrying cylinder at start (69.5 m), with 2 T toroidal field at 1 cm and with absorbers 10 cm thick at center, 8 cm at pipe radius. Figures on **right** refer to 1.25 T, 30 cm radius solenoidal channel with 12 cm radius of current carrying cylinder at start (69.5 m), with 2.5 T toroidal field at 1 cm and with flat 10 cm thick absorbers.

a spurious component from 'misplacing' the (E–t)-window. Care must also be taken to distinguish cooling from mere collimation, i.e., when reduction in phase space volume is mostly due to reduction in muons captured.

4 Concluding Remarks

The simulations presented here suggest one can achieve an 'accepted' muon yield at the exit of the decay channel of about half the combined number of pions and muons at its entrance. Placing a set of absorbers—and compensating acceleration—in the decay channel, downstream from where most pions have decayed, reduces phase space volume significantly in the narrow channel case. Six dimensional phase space of the muons is reduced by more than a factor of three, at a cost of about 13% in yield. For the wide channel case absorbers cut muon yield by more than half while phase space volume actually increases somewhat. A supplemental toroidal field—applied at larger radii only and where absorbers are present—is beneficial in either case. In the narrow channel it restores some of the losses associated with the absorbers and shrinks transverse size of the bunch by about 30% while leaving phase space unaltered. For the wide channel case the toroidal field doubles muon yield while ϵ_6 is reduced by 45% and *rms*

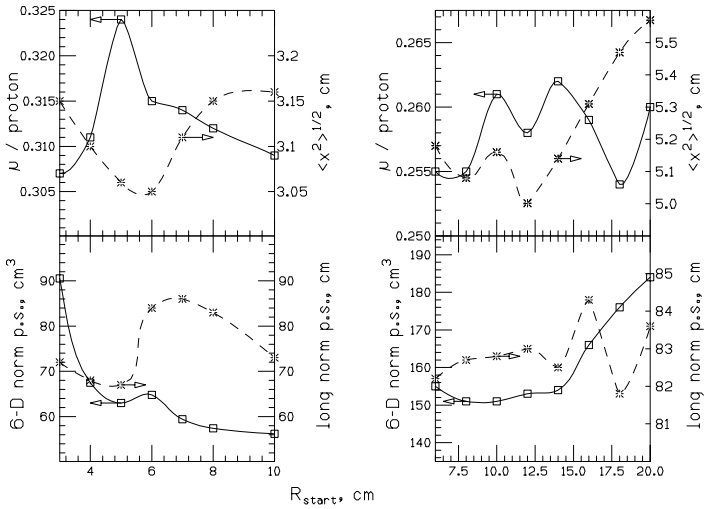

Figure 15: (**top**) Number of muons captured (*left scale*), *rms* radius (*right scale*) and (**bottom**) normalized 6-D (*left scale*) and longitudinal phase space (*right scale*) vs radius of current carrying cylinder at start. Figures on **left** refer to 5 T, 15 cm radius solenoidal channel with current carrying cylinder of 2 cm radius at exit (146.4 m), with 2 T toroidal field at 1 cm and with absorbers 10 cm thick at center, 8 cm at pipe radius. Figures on **right** refer to 1.25 T, 30 cm radius solenoidal channel with current carrying cylinder of 6 cm radius at exit (146.4 m), with 2.5 T toroidal field at 1 cm and with flat 10 cm thick absorbers.

transverse size is more than halved. This smaller beam size facilitates exiting the decay channel. A toroidal field of 2 T referenced at 1 cm present outside of r_{cyl}=5 cm at the start of the absorbers and reduced to r_{cyl}=2 cm at exit is close to optimum for the 15 cm/5 T channel. Comparable figures for the 30 cm/1.25 T channel are: a field of 2.5 T, referenced at 1 cm, r_{cyl}=12 cm at the start and 6 cm at exit. It must be emphasized that the optimization performed here is rather cursory in view of the large parameter space and that—at this stage—no clear cut definition of what is optimum exists. The above optimization uses the conventional $N_\mu^2/\sqrt{\epsilon_6}$ criterion. Typically, this exhibits a broad maximum in the vicinity of the parameters quoted above. In practice, implementing a toroidal field of the magnitude envisioned here, in the presence of a solenoidal field and RF cavities, may pose considerable difficulties which have yet to be addressed. Providing such a field may require compromises in the rest of the design, e.g., in the quality of the solenoidal and RF fields, leading to a new round of optimizations.

Future simulations can improve the above estimates. The results presented above are not to be interpreted as claims on new and improved methods until confirmed by more thorough simulations. Most notably, the spatial distribution of magnetic and RF fields must be made more realistic. Beam energies are likely

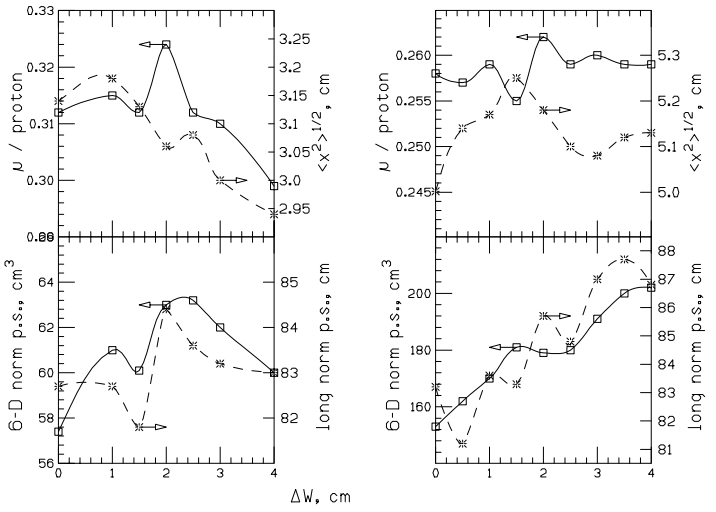

Figure 16: (**top**) Number of muons captured (*left scale*), *rms* radius (*right scale*) and (**bottom**) normalized 6-D (*left scale*) and longitudinal phase space (*right scale*) vs difference in thickness of absorbers 10 cm thick at center, less than that by ΔW at pipe radius. Figures on **left** refer to 5 T, 15 cm radius solenoidal channel with current carrying cylinder of 5 cm radius at start (69.5 m), 2 cm at exit (146.4 m), with 2 T toroidal field at 1 cm. Figures on **right** refer to 1.25 T, 30 cm radius solenoidal channel with current carrying cylinder of 12 cm radius at start (69.5 m), 6 cm at exit (146.4 m), with 2.5 T toroidal field at 1 cm.

somewhat higher than optimal and RF gradients are somewhat higher than can be readily developed at these low frequencies. The material presence of wires or cylinder associated with the toroidal field—and changes in shape of the absorbers to mitigate the presence of the wires—must be explicitly included in the simulation. The pion interaction model adopted here does not treat pion production and should be replaced by one with wider range of applicability. While it is tempting to further pursue optimization of the various parameters with the present code it would perhaps be better to first introduce at least some of the above refinements. Solenoidal field and diameter of the collection channel, possibly along with a toroidal field, should also be a part of the optimization. Because of the length of the channel this will have a large impact on economic feasibility.

The change in angular momentum, and its effect on the emittance, upon leaving the decay channel should be further investigated—along with schemes to minimize it. The muons within the channel possess an angular momentum associated with their Larmor motion which is matched to that of the solenoid. Upon leaving the solenoid the radial fields impart an opposite angular momentum which cancels—to first order—that due to longitudinal field. However, when aborbers are present the angular momentum is gradually reduced

($L_z = L_{z,0} exp(-\Delta p/p)$ where Δp is the momentum loss in the absorbers) which destroys the cancellation. The beam thus acquires net angular momentum—and increased emittance—when leaving the solenoid unless measures are taken to explicitly remove this angular momentum. The main effect of the toroidal fields with respect to beam angular momentum is the reduction in transverse size of the beam which lessens the emittance dilution encountered at the exit (since $\Delta\epsilon_x \propto x^2$ [11]). When ionization cooling is provided by a system of lithium– or other toroidal lenses [12], one possibility is to place a large diameter, relatively high field lens within, partly within, or immediately downstream of the decay channel. This could further reduce beam size and the strong toroidal field will tend to dominate the solenoidal fringe fields thus mitigating their disruptive effects. Alternatively one may consider a continuation of the channel with progressively increasing toroidal fields at smaller radii to further cool the beam and reduce its size. It is hoped that further investigations into these matters will not totally negate the promising results obtained so far (along with any benefits resulting from a more thorough optimization).

Finally, the collection channel must be integrated with the rest of the muon collider complex. Different target systems—such as those composed of heavier nuclei or tilted with respect to the channel axis—as well as different driver beams (e.g, change in energy and/or beam size or projectiles other than protons) produce pions in different numbers and phase space characteristics which may have significant effects on parameter optimization in the decay channel. Likewise, rival ionization cooling schemes will differ in their capability to accommodate beam delivered by the decay channel, which will influence the optimization of the phase rotation channel.

Our thanks to A. Moretti for useful discussions.

References

[1] see e.g., $\mu^+\mu^-$ *Collider. A Feasibility Study*, BNL-52503, FNAL-Conf-96/092, LBNL-38946 (1996).

[2] N. V. Mokhov, *The* MARS *Code System User's Guide, version 13 (95)*, FNAL-FN-628 (1995). MARS files are courtesy of N. Mokhov.

[3] A. N. Skrinsky and V. V. Parkhomchuk, Sov. J. Nucl. Phys. **12**, 3 (1981); E. A. Perevedentsev and A. N. Skrinsky, Proc. 12th Int. Conf. on High Energy Accel., 485 (1983); D. Neuffer, Particle Accelerators **14**, 75 (1983); D. Neuffer, Proc. 12th Int. Conf. on High Energy Accel., 481 (1983); D. Neuffer, Nucl. Inst. Meth. **A350**, 27 (1994).

[4] N. V. Mokhov, R. J. Noble and A. Van Ginneken, Fermilab-CONF-96/006.

[5] A. Van Ginneken, Nucl. Inst. Meth. **A362**, 213 (1995).

[6] D. Ashery et al., Phys. Rev. **C23**, 2173 (1981).

[7] *Review of Particle Properties*, L. Montanet et al., Phys. Rev. **D50**, 1177 (1994).

[8] N. Metropolis et al., Phys. Rev. **110**, 204 (1958).

[9] G. Bellettini et al., Nucl. Phys. **79**, 609 (1966).

[10] R. M. Sternheimer, M. J. Berger and S. M. Seltzer, Atomic Data and Nuclear Data Tables **30**, 261 (1984).

[11] R. K. Cooper, Particle Accelerators **7**, 41 (1975).

[12] D. Neuffer and A. Van Ginneken, Nucl. Inst. Meth. **A403**, 1 (1998).